Specific Absorption Rate Studies of the Parallel Transmission of Inner-Volume Selective Excitations at 7 Tesla

A. C. Zelinski[1], L. M. Angelone[2], V. K. Goyal[1], G. Bonmassar[2], E. Adalsteinsson[1,3], and L. L. Wald[2,3]

[1]Research Laboratory of Electronics, MIT, Cambridge, MA, United States, [2]Martinos Center for Biomedical Imaging, MGH, Charlestown, MA, United States, [3]Harvard-MIT Division of Health Sciences & Technology, MIT, Cambridge, MA, United States

Introduction. SAR is a major concern in the parallel transmission (pTX) of spatially-tailored 2D and 3D excitation pulses due to *E* field superposition that occurs when driving multiple channels concurrently, and the possible inefficiency of producing excitations via regional cancellation. Here, we study average and local SAR in a head model at 7 Tesla for 2D spiral-trajectory inner-volume excitation pulses on an 8-channel pTX array. Excitation fidelity [normalized root-mean-square error (NRMSE) with respect to the desired excitation] is held constant and SAR is analyzed as a function of target flip angle, position, size, smoothness, orientation, and trajectory undersampling (acceleration) factor, *R*.

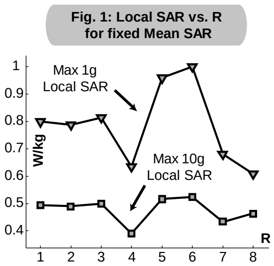

Fig. 1: Local SAR vs. R for fixed Mean SAR

Methods. We use FDTD methods at 300 MHz in a human head model [1] to derive the *E* & *B* fields for each coil at locations **r** per Amp. of current in an array of eight, 15_{cm}-dia. overlapping loops spaced by 45^o on a 28_{cm}-dia. cylinder. B_1^+ fields are formed and used in a Bloch equation simulator to model pTX excitations.

Pulse design. We design pulses to form approximations of a box-shaped "inner volume" target excitation with 0^o flip outside the box; the target is a 15^o-flip, centered, $28_{mm}\times 28_{mm}$ square (unless specified otherwise). Trajectories are 2D spirals, radially undersampled by factors of *R* relative to the original FOV. First, the linearized formalism in [2] is used to generate matrices & vectors. Then, for a given target magnetization, $d(\mathbf{r})$, we form $\mathbf{d}_{in} \in \mathcal{C}^{M\mathrm{in}}$ and $\mathbf{d}_{out} \in \mathcal{C}^{M\mathrm{out}}$. Within-square pixels make up $\mathbf{d}_{in}$ and all equal 15°, whereas $\mathbf{d}_{out}$ contains out-of-square, zero-flip-angle pixels. Pulses are designed by solving $\min_{\mathbf{b}} \{\|\mathbf{W}(\mathbf{d}\text{-}\mathbf{Ab})\|_2^2 + \lambda\|\mathbf{b}\|_2^2\}$, where $\mathbf{d}=[\mathbf{d}_{in}^T,\mathbf{d}_{out}^T]^T$, $\mathbf{A}=[\mathbf{A}_{in}^T,\mathbf{A}_{out}^T]^T$, $\mathbf{W}$ is diagonal, & $\mathbf{W}_{ii} = \alpha$ if $i = 1,\ldots,M_{in}$ and 1 otherwise (i.e., in-square & out-of-square differences are weighted by α & unity, respectively). A search over (α, λ) finds **b** such that in-box NRMSE, $e_1 = \|\mathbf{d}_{in}\text{-}\mathbf{A}_{in}\mathbf{b}\|_2/\|\mathbf{d}_{in}\|_2$, is 15±1%, and overall NRMSE, $e_{tot} = \|\mathbf{d}\text{-}\mathbf{Ab}\|_2/\|\mathbf{d}\|_2$, is 40±1%. This novel approach ensures *both* in-square & overall error are reasonable; otherwise, designing only for fixed e_{tot} causes e_1 to vary widely across *R*.

SAR calculation. For each pulse, vector-sum *E* field squared-magnitudes are time-averaged; spatial SAR integrals are computed using the conductivities and densities of the head model to obtain whole-head and maximum local 1-gram & 10-gram averaged SAR. Here, the effect of the acceleration factor is explicitly accounted for: e.g., $R = 1$ pulses are assumed to have 100% duty cycle, whereas $R = 4$ pulses a 25% duty cycle. SAR differences across *R* will thus reflect only the extra power needed to maintain target fidelity.

Results & Discussion. Figs. 1-5 show log-scaled mean & local SAR along with simulated excitation patterns for $R = 4$. Excitation fidelity is reported and is kept nearly constant across the comparisons as intended. All figures show sizable SAR increases with *R*. With this 8-ch array, there appears to be a consistent "jump" in SAR across all experiments as *R* transitions from 4 to 5.

Fig. 1: Local SAR vs. *R* for fixed mean SAR. For all *R*, the square's flip angle is varied & pulses are designed until mean SAR equals 0.15±0.01 W/kg. The ratio of local to mean SAR defined in this way is not monotonic with *R*.

Fig 2: SAR vs. target position. As a function of box position, there is a qualitative difference in SAR growth with *R*: for R ≤ 4, centered squares (i.e., when $x_0 = 0$) have the lowest SAR, whereas for R > 4, their SAR is the highest.

Fig. 3: SAR vs. target size. SAR growth differences are also apparent here. For $R \geq 5$, SAR drops significantly with size, yet for $R < 5$, it grows rapidly. Thus for large *R*, exciting large regions actually costs less in terms of SAR.

Fig. 4: SAR vs. target smoothness. SAR decreases significantly with the smoothness of the target, suggesting that sharp edges are costly in terms of SAR. Smoother excitations generate significantly lower mean and local SAR.

Fig. 5: SAR vs. orientation. For $R > 4$, spikes in SAR occur at some orientations. In general, the worst-SAR cases (e.g., $R = 6$, rotation = 45°) are those where the box is highly asymmetric with respect to the shape of the head.

Fig. 2: SAR as a function of target spatial offset

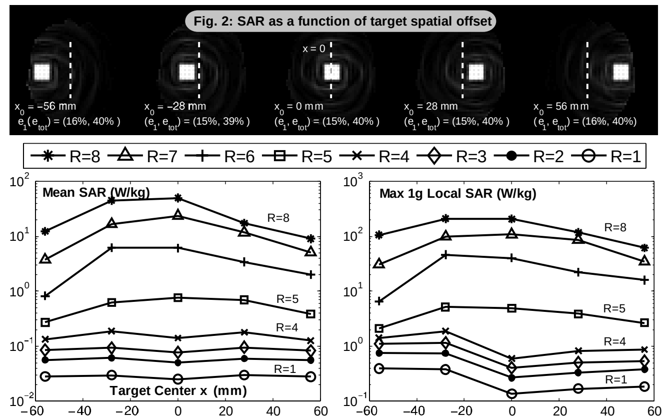

Fig. 3: SAR as a function of target size

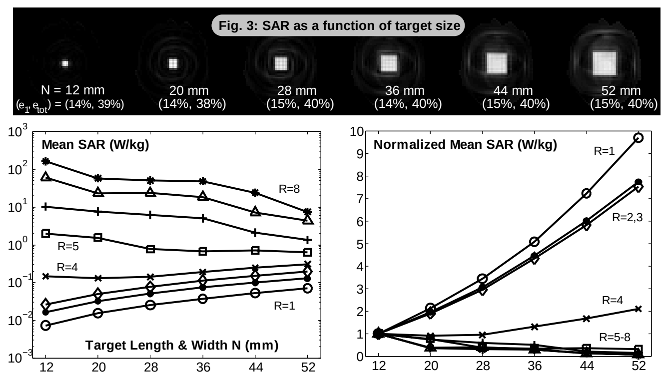

Fig. 4: SAR as a function of target smoothness

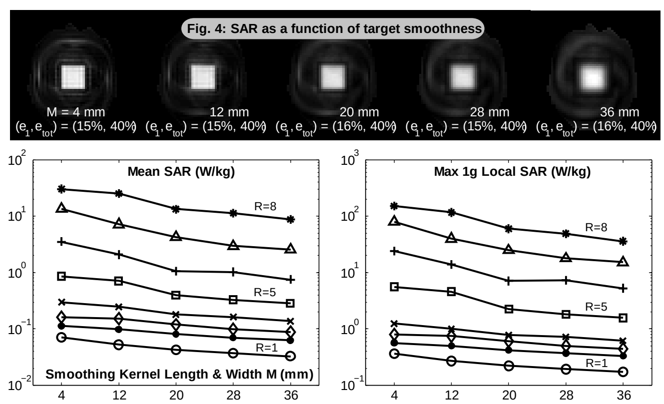

Fig. 5: SAR as a function of target orientation

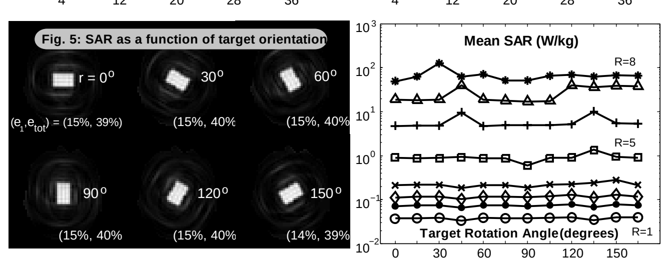

References. [1] N. Makris & D. Kennedy, 29-Tissue High-Resolution Head Model, Center for Morphometric Analysis, MGH; [2] Grissom et al. MRM '06;56(3):620-629.